



# Synthesis and Electrical Characterization of Lead-Free Electronic Material: $\text{Bi}(\text{Co}_{2/3}\text{Nb}_{1/3})\text{O}_3$

S. Halder<sup>1</sup> · S. Bhuyan<sup>1</sup> · R. N. P. Choudhary<sup>1</sup>

Received: 8 June 2018 / Revised: 8 October 2018 / Accepted: 21 October 2018 / Published online: 26 October 2018  
© The Korean Institute of Electrical and Electronic Material Engineers 2018

## Abstract

A lead-free electronic compound with chemical composition  $\text{Bi}(\text{Co}_{2/3}\text{Nb}_{1/3})\text{O}_3$  has been synthesized via classical solid state reaction based ceramic technology. The structure of the compound as well as the frequency and temperature field dependent resistive, conductive and dielectric properties of the specimen have been examined. The room temperature X-ray diffraction analysis exhibits the formation of the sample in orthorhombic crystal symmetry. The observed dielectric constant and tangent loss characteristics substantiate the prepared compound as a dielectric. The impedance spectra confirms the presence of negative temperature coefficient of resistance behaviour, grain and grain boundary effect in the fabricated compound. The compound modulus spectrum shows that the temperature dependent conductivity relaxation phenomenon is of non-exponential-type. The illustrated important characteristics props up the material for different device applications.

**Keywords** X-ray diffraction · Dielectric · Impedance analysis · Conductivity

## 1 Introduction

Nowadays, material scientists have focussed their attention on the design and development of new innovative compounds with exceptional properties needed for fabrication of modern devices. Some dielectric materials, especially, have gained much attention in recent years by various researchers all over the globe for different industrial applications, such as waveguides, microstrip, antennas, dielectric resonators, etc. [1–4]. Such type of dielectric materials in ceramics form with perovskite structure is found to be one of the interesting materials for higher frequency applications. Several research groups have ascertained that several perovskite materials are considered as smart materials for variety of applications. Perovskite structures have a wide diversity of structural transformation and properties. It has been observed that some compounds having perovskite structure show different physical and electrical properties useful for different technological application [5–8]. The general formula of a perovskites structure is  $\text{ABO}_3$ , where A is normally mono

or divalent and B is tri-hexavalent ions. An ideal perovskite structure consists of larger A cations (12-fold coordinated by oxygen) and smaller B cations (surrounded by sixfold coordinated octahedral anions). It has been also found that some lead-based perovskite systems, such as lead zirconate titanate ( $\text{Pb}(\text{ZrTi})\text{O}_3$  (PZT), lead magnesium niobate  $\text{Pb}(\text{Mg}_{1/3}\text{Nb}_{2/3})\text{O}_3$  (PMN), lead zinc niobate  $\text{Pb}(\text{Zn}_{1/3}\text{Nb}_{2/3})\text{O}_3$  (PZN), are commonly used for a wide ranging applications because of their exceptional electronic, electro-optic pyroelectric, dielectric and piezoelectric properties [9–11]. These lead based device materials contain up to 60 wt% of PbO which imposes toxic and negative effect on both ecology and human beings. The toxicity of lead oxide and higher vapor pressure during high temperature processing have stimulated a high demand to find alternative eco-friendly compounds. So a significant awareness has been drawn by the industrial and scientific society to develop (synthesize, design, characterize) non-lead compounds for spintronic devices, multiple state memories, magnetic sensors etc. [12–14]. Recently, discovery of bismuth compounds, namely  $\text{BiFeO}_3$ ,  $\text{BiMnO}_3$ ,  $\text{Bi}(\text{Mg}_{1/2}\text{Ti}_{1/2})\text{O}_3$  based perovskite compounds have drawn the attention of scientists due to their intrinsic versatility by chemical manipulation. Generally, Bi-based compounds are unique due to their dormant behaviour toward electrodes, low firing and sintering temperature (800–950 °C) with high densification in texture which

✉ S. Halder  
sarbasrihalder@gmail.com

<sup>1</sup> Department of Electronics and Communication Engineering, ITER, Siksha 'O' Anushandhan (Deemed to be University), Bhubaneswar 751030, India

make them suitable for various applications. The electronic structure of eco-friendly ( $\text{Bi}^{3+}$ ) is similar with Pb as lead is located behind bismuth in the periodical table with a electron configuration of both elements as ( $6s^2, 6p^0$ ). Therefore, lead can be replaced by bismuth during fabricating of perovskite compound. In recent years, scientists and engineers have focused their attention to find and synthesize compounds that can sustain high temperature so that they can be used in future for numerous high temperature applications [15, 16]. For capacitive application, a compound with high permittivity, lower loss (that can persist high temperature) are needed for using it as a capacitor. Some Bi-based compounds, such as  $\text{Bi}(\text{Zn}_{1/2}\text{Ti}_{1/2})\text{O}_3$  [1],  $\text{BiScO}_3$  [2],  $\text{BiScO}_3\text{--Bi}(\text{Zn}_{1/2}\text{Ti}_{1/2})\text{O}_3$  [3], and  $\text{BiScO}_3\text{--}(\text{Bi}_{1/2}\text{K}_{1/2})\text{TiO}_3$  [4], show some interesting properties for the high temperature capacitor [17–20]. Some tantalum (Ta) based compounds, such as  $\text{Ba}(\text{Zn}_{1/3}\text{Ta}_{2/3})\text{O}_3$  (BZT) usually have lower temperature coefficient of resonant frequency, higher dielectric constant, lower dissipation factor for which they are generally used for different applications. The higher cost of tantalum oxides has called for search of other such similar, cost effective compounds, such as analogues-niobium based systems.

The present work is motivated by the idea of synthesizing eco-friendly compound that can even function at higher temperature and frequency. The main limelight of the present study is the development of niobium based perovskite compound  $\text{Bi}(\text{Co}_{1/3}\text{Nb}_{2/3})\text{O}_3$  (BCN) which has a lower sintering temperature. Bismuth occupies the A site and the B site is occupied by cobalt and niobium. Co is a well known ferromagnetic material which is nowadays extensively used for applications, like in gas sensors, lithium batteries, data storage etc. Through literature review, it is also estimated that not much information regarding detailed electrical and dielectric characterization of lead-free BCN compound is available. Therefore, in the present communication, we report our comprehensive study of structural feature, electrical (capacitive and resistive behavior), impedance and dielectric properties of a newly synthesized  $\text{Bi}(\text{Co}_{1/3}\text{Nb}_{2/3})\text{O}_3$  using a high temperature solid state method. Standard characterization techniques were used for the study of the material.

## 2 Experimental Details

$\text{Bi}(\text{Co}_{2/3}\text{Nb}_{1/3})\text{O}_3$  was prepared through a cost effective standard high-temperature solid-state reaction route using highly-pure (> 99.5%) oxide and carbonate powders;  $\text{Bi}_2\text{O}_3$ ,  $\text{CoCO}_3$ , and  $\text{Nb}_2\text{O}_5$  (M/S LOBA Chemical, India). The ingredients were weighted in stoichiometric proportion by using a digital electronic balance (Mettler Type: New Classic MF; Model: ML204/A01). To obtain fine mixed powder, the above ingredients were mixed in a dry

grinding mode for 2 h, and then in wet grinding mode using methanol for 4 h in an agate mortar. The homogeneous powder was then put into high-purity alumina crucible for calcinations at an optimised temperature of 800 °C in a high-temperature programmable furnace for a duration of 8 h. The phase-purity of the calcined material was checked by using the diffraction (data and profile) obtained from XRD diffractometer (Rigaku Smart Lab). The diffraction analysis was done at scanning rate of 2°/min for Bragg angle (angle range of  $20^\circ \leq \theta \leq 70^\circ$ ) to confirm the formation and structural data of the synthesized sample. The peaks of XRD spectrum were indexed and the structural parameters of the prepared compound were obtained using the computer program package (POWD) version 2.2. By using hydraulic press the calcinated powder was then compressed to fabricate disk-shaped pellets by mixing polyvinyl alcohol (binder) with the calcined powder. At a temperature higher than calcined temperature (i.e., 820 °C), the pellets were sintered in furnace for a duration of 12 h. To measure the electrical properties (conductivity, dielectric, impedance, modulus) of sintered sample both the faces of the compacted pellet was made smooth and then it was painted with silver paste for making the surface conducting. For measuring the electrical, pellets were by firing the samples. The LCR meter (model PSM 1735, N4L) was used to record the electrical parameters of the compound at selected temperature (150–450 °C) and frequency ( $10^3\text{--}10^6\text{Hz}$ ). Along with the LCR meter a laboratory fabricated sample holder and vertical pit furnace is used in the experimental setup. The temperature was displayed by a digital panel meter (Rishabh N25) which was measured by a chromel–alumel thermocouple (AK-type). For the electrical characterization the specimen (pellet) was placed in the sample holder in between two electrodes made of silver/aluminum in the configuration of aluminum plate/silver paste/sample/silver paste/aluminium plate. The sample holder was then kept in the vertical pit furnace that was connected with the LCR meter (PSM1735). The experimental equipment used here comprises of a Impedance Analyser (Newtons 4th Limited, UK) that has been interfaced to a measurement unit NumetriQ Phase Analyser Multimeter (PSM1735). The NumetriQ (PSM1735) consists of dual input channels for voltage and current measurement and a single output channel. It also consists of dual processors: CPU (central processing unit) used for controlling and display and DSP (Digital signal processor) used for analyzing data. The NumetriQ uses DFT analysis to measure the real and imaginary components of current ( $a + jb$ ) and voltage ( $c + jd$ ) at the fundamental frequency. The complex impedance  $Z = \frac{v}{i} = \frac{c+jd}{a+jb}$  can be calculated from the complex voltage and current. The different electrical parameters (Q-factor both imaginary and real),

tangent loss (real/imaginary), capacitance, inductance, resistance, etc.) can be analyzed by the help of complex impedance.

### 3 Experimental Results

#### 3.1 Structural Study

Figure 1 displays the room temperature XRD spectrum of calcined powder of  $\text{Bi}(\text{Co}_{2/3}\text{Ta}_{1/3})\text{O}_3$ . This pattern helps to identify the structural parameters and phase-purity of the synthesized sample. The formation of compound can be suggested by analysing reflection peaks which are not similar to those of its ingredients. By indexing all the XRD peaks using commercial available program ‘POWD’, the structure of the compound was analysed with Bragg angle ( $2\theta$ ) and peak intensity in different crystal systems and cell configuration [21]. By observing the good fit between calculated and observed values of  $d$  (inter-planar spacing) of each reflection an orthorhombic crystal system was selected. The least-squares lattice parameters of the chosen unit cell (after refinement) were found to be:  $a = 9.0805$  (40) Å,  $b = 7.5283$  (40) Å,  $c = 8.6778$  (40) Å (figure in parenthesis is estimated standard deviation). After normalization, unit cell dimension can be considered as distorted perovskite.

The average crystalline/particle size ( $P$ ) was calculated by enlarging some broadly spread (over Bragg angles) powerful and medium reflections in the Scherrer’s relation:  $P_{hkl} = k \lambda / \beta_{1/2} \cos \theta$  [22] where  $k$  (constant) = 0.89,  $\lambda = 1.5405$  Å and  $\beta_{1/2}$  = full width at half maximum (in radians). The  $P_{hkl}$  (crystallite size) was found to be 70 nm.

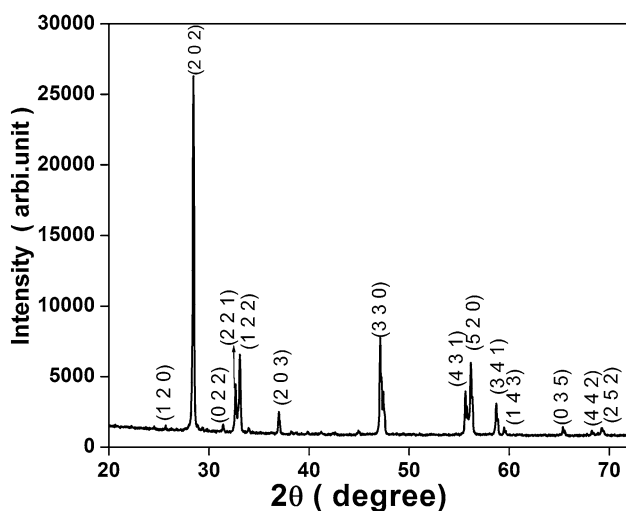


Fig. 1 XRD pattern of  $\text{Bi}(\text{Co}_{2/3}\text{Ta}_{1/3})\text{O}_3$

#### 3.2 Dielectric Analysis

The temperature and frequency dependent dielectric properties [dielectric constant ( $\epsilon_r$ ), tangent loss ( $\tan \delta$ )] of the synthesized specimen can be studied using dielectric spectroscopy. The circular pellet is inserted in between two electrodes made of silver and then placed in the sample holder for the measurement of the insulating and resistive properties of the synthesized specimen. The experimental setup is used to measure the  $\tan \delta$  and parallel capacitance values that are used to calculate the dielectric constant of the sample using the relation:  $\epsilon_r = \frac{C_p d}{\epsilon_0 A}$ , where  $C_p$  = parallel capacitance,  $A$  = area of specimen,  $d$  = thickness of specimen and  $\epsilon_0$  = permittivity of free space. The synthesized material  $\epsilon_r$  (dielectric constant) and  $\tan \delta$  (tangent loss) variation with temperature over selected range of frequency is shown in Fig. 2a, b. The  $\epsilon_r$  as well as  $\tan \delta$  follows the similar trend like other dielectric compounds (i.e., inversely dependent with frequency). In the region of high frequency, the  $\epsilon_r$  value of the compound decreases while in the lower-frequency region, the material has a high value of  $\epsilon_r$  that can be due to the electrons accumulation caused by space charge polarization. With the ascend in temperature, the  $\epsilon_r$  was seen to rise gradually until it attains its maximum value ( $\epsilon_{max}$ ), and then on further rising of temperature, the  $\epsilon_r$  increases rapidly. This trend of  $\epsilon_r$  can be seen at high temperatures that may be due to the movement of space charges (oxygen vacancies), created at the sintering process [23]. It can be noticed in loss ( $\tan \delta$ ) spectrum that at room temperature the  $\tan \delta$  value is low while in the region of high temperature, the loss tangent increases which can be revealed by hopping phenomena of charge carriers as it is extremely persuaded by  $\tan \delta$  peak [24]. The vacancy or defects (mixed dislocation, stacking

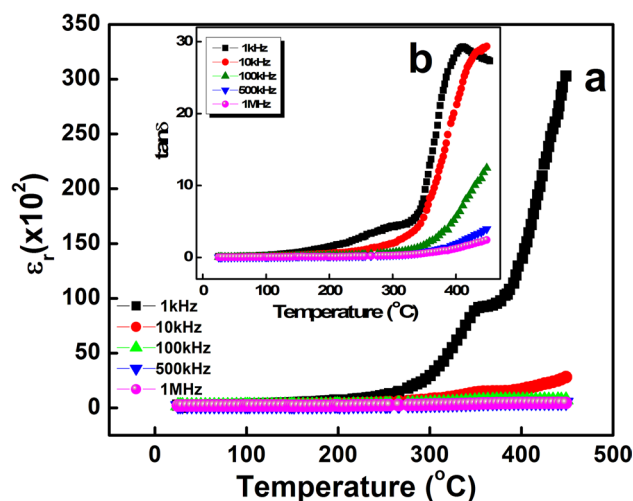


Fig. 2 Temperature dependence of dielectric constant and tangent loss at selected frequencies of  $\text{Bi}(\text{Co}_{2/3}\text{Nb}_{1/3})\text{O}_3$

faults and planner), the distribution of charge carriers and/or presence of a unknown impurity phase cause the alteration in the loss factor at high temperatures. At the high temperatures, the loss tangent decreases quickly with rise in frequency, while it increases sharply in the region of lower frequency [25]. The  $\epsilon_r$  and  $\tan \delta$  of the fabricated compound at a temperature of 450 °C and a frequency of 10 kHz is 3300 and 30 respectively.

### 3.3 Impedance Properties

CIS (complex impedance spectroscopy) is a useful mechanism to determine the electrical conduction mechanism of the synthesized compound and to analyze the movable carriers in bulk or interfacial regions. This technique helps to visualize the effects of bulk, grain boundary and electrode in the compound. The electrical properties of the specimen is normally displayed in terms of permittivity ( $\epsilon^*$ ), tangent loss ( $\tan \delta$ ) and complex impedance ( $Z^*$ ), complex admittance ( $Y^*$ ), modulus ( $M^*$ ), which are too related with one another. The  $Z^*$  (real and imaginary parts) are measured using some basic equation:

$$\text{Complex permittivity: } \epsilon^* = \epsilon' - j\epsilon'' \tag{1}$$

$$\text{Loss tangent: } \tan \delta = \frac{\epsilon''}{\epsilon'} = -\frac{z'}{z''} = \frac{M''}{M'} \tag{2}$$

$$\text{Complex impedance: } z^* = z' - z'' = R_s - \frac{j}{\omega C_s} \tag{3}$$

$$\text{Complex admittance: } Y^* = Y' + Y'' = \frac{1}{R_p} + j\omega C_p \tag{4}$$

$$\text{Complex Modulus: } \frac{1}{\epsilon^*} = M^* = M' + jM'' = j\omega C_o Z^* * \omega \tag{5}$$

$$M' = -\omega C_o Z \quad \text{and} \quad M'' = \omega C_o Z' \tag{6}$$

The complex impedance (real and imaginary) part is illustrated by the following equation:

$$Z' = \frac{R}{1 + (\omega\tau)^2} \quad \text{and} \quad Z'' = \frac{\omega R\tau}{1 + (\omega\tau)^2} \tag{7}$$

The frequency dependent complex impedance real part ( $Z'$ ) at different temperatures is displayed in Fig. 3a, b. The plot shows that  $Z'$  declines with increase in temperature that signifies a rise in its conductivity. In the lower-frequency zone the decrease in the magnitude of  $Z'$  indicates the negative temperature coefficient of resistance (NTCR) behaviour of the sample.  $Z'$  spectrum merges at high frequency region that may be due to liberation of space charge [26]. The resonance frequency (i.e. frequency linked to  $Z''$  of the applied

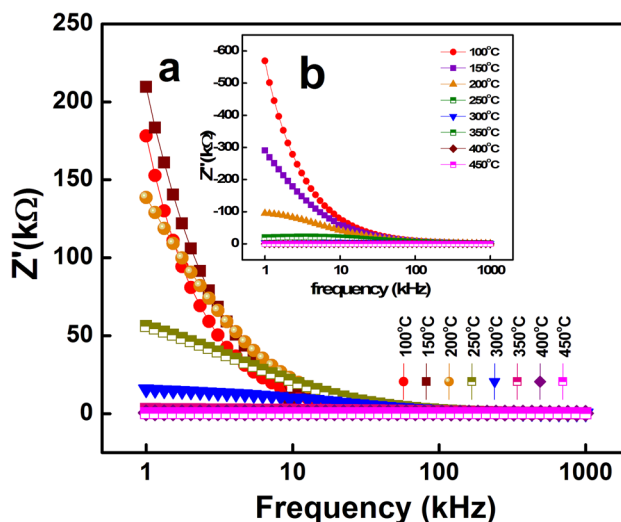


Fig. 3 a, b Real and imaginary part of complex impedance spectra at selected temperatures and frequency. c Variation of  $Z'$  with  $Z''$  as a function of temperature

electric field) is reliant on composition and temperature of the synthesized compound. The static charges and vacancies that vary with temperature cause resonant frequency dependent relaxation mechanism in the specimen [27]. Figure 3b illustrates the impedance imaginary ( $Z''$ ) part of BCN variation with frequency at selected temperatures. It can be noticed that with rise in temperature imaginary peaks with asymmetric broadening moves toward the higher side of frequency and the spectra merges there. The asymmetric peak broadening indicates presence of multiple relaxation times with increase in temperature.

Figure 3c displays the Nyquist diagram of the synthesized compound at selected range of temperatures (100–450 °C) and frequency ( $10^3$ – $10^6$ Hz). With the rise in temperature the occurrence of semicircular arc in the Nyquist plots, characterizes the impedance that can be allocated to the grain, grain boundary and/electrode effects. The center of the plot lies below the real axis (depressed semicircular arc) due to imperfections in most of the solids at higher temperature which entitles non-Debye type of relaxation phenomenon. For Debye type relaxation the semicircular arc centre lies on the real  $Z$  axis. The movement to non-Debye type relaxation from the Debye type can be characterized by an equivalent circuits built up by a (CPE) Q constant phase element with parallel RC circuit. It can be noticed that the semicircular arc in the nyquist plot shows some depression thus indicating the presence of non-Debye type (semicircle arc centre moves below the X-axis) of relaxation mechanism [28]. The existence of a single semicircular arc up to a temperature of 150 °C reveals that within this selected range of temperature the compound shows single conduction process/Bulk (grain) effect and it is not affected by grain boundary. This

grain effect is illustrated by an electrical circuit consisting of a parallel connection of  $R_b$  and  $C_b$  with constant phase element (Q). But at higher temperature above 150 °C the semicircular arc tends to form second semicircle in the plot thus confirms that the electrical process in the sample arise due to the contribution from grain and grain boundary effect. From the Nyquist plot it can be indicated that the material comprises of two semicircles one due to grain and second one due to grain boundary. By using a commercial software ZSimpWin” the experimental data is fitted with an electrical circuit model and we obtained the values of grain and grain boundary R, Q, C as shown in Table 1. The grain resistance ( $R_b$ ), grain capacitance ( $C_g$ ), grain boundary resistance ( $R_{gb}$ ), grain boundary capacitance ( $C_{gb}$ ) can be evaluated from the intercept of the semicircular arcs.

### 3.4 Ac Conductivity Analysis

Figure 4 shows the AC conductivity plot variation with frequency of BCN. The dielectric data is used for calculating the electrical conductivity value by following the below relation:

$$\sigma_{ac} = \omega \epsilon_r \epsilon_0 \tan \delta \tag{8}$$

where  $\epsilon_r$ =relative dielectric constant,  $\omega$ =angular frequency,  $\tan \delta$ =tangent loss,  $\epsilon_0$ =permittivity of free space.

The plot exhibits dispersion towards the region of higher temperature around selected range of frequency. From the graph it can be estimated that with rise in frequency conductivity increases while it remains constant at lower frequency value (hopping frequency). This conductivity plot also shows temperature dependent behavior as on increasing the value of temperature, it tends towards the high frequency. In the synthesized compound electrical conduction mechanism dependent on frequency is a hopping type, which obeys the Jonscher’s power relation [29]:

$$\sigma_{ac} = \sigma_{dc} + A\omega^n \tag{9}$$

where  $\sigma_{dc}$  is the dc conductivity, A is a temperature dependent pre-exponential factor/constant and n is an exponent

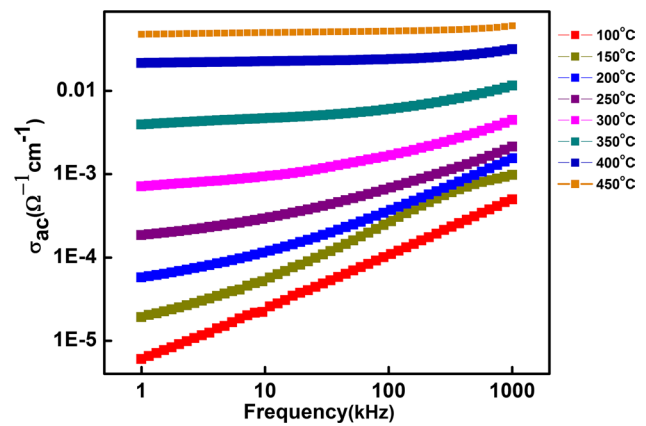


Fig. 4 Frequency dependent AC conductivity spectrum at selected temperature (100–450 °C)

which lies between  $0 \leq n \leq 1$ . With the rise in temperature, the A generally increases while the exponent n shows a reverse trend that can be noticed from conductivity spectrum. As the value of n is less than one and it declines with rise in temperature it can be signified that the thermally activated conduction mechanism is of non-Debye type. At higher frequencies the conductivity enhances with the temperature that may be due to the decrease in barrier properties of the compounds.

Figure 5 illustrates the plot of ac conductivity versus absolute inverse temperature at different frequency. With the ascend in frequency it can be seen that the conductivity increases which signifies the dispersion of conductivity with frequency whereas a view of narrowing of dispersion in conductivity with ascend in temperature can be estimated by observing the merging of all the ac conductivity curves at the higher range of temperatures. The AC conductivity analysis dependent on temperature and frequency is used to calculate the activation energy while following the Arrhenius relationship:

$$\sigma_{dc} = \sigma_0 \exp(-E_a/k_B T) \tag{10}$$

where the Boltzmann constant is  $k_B$ ,  $\sigma_0$  is pre-exponential factor and  $E_a$  is the activation energy. The  $E_a$  is calculated

**Table 1** Fitting parameters of Bulk and grain boundary resistance as well as capacitance of impedance parameters of the compound  $\text{Bi}(\text{Co}_{2/3}\text{Nb}_{1/3})\text{O}_3$

Temperature (°C)	$R_g$ (Ω)	$C_g$ (F)	CPE	$R_{gb}$ (Ω)	$C_{gb}$ (F)	CPE <sub>gb</sub>
100	8.146E+006	1.404E-010	2.040E-009	–	–	–
150	1.084E+006	9.802E-011	2.831E-009	–	–	–
200	1.782E+005	1.426E-010	7.738E-009	9.603E+004	3.029E-009	–
250	7.400E+004	1.492E-010	3.854E-008	9.806E+003	3.490E-008	–
300	1.732E+004	1.612E-010	7.589E-008	6.107E+003	1.001E-007	–
350	7.439E+002	1.586E-011	1.234E-006	2.650E+003	1.307E-010	4.896E-008
400	3.529E+015	2.856E-010	3.685E-003	4.045E+002	1.363E-016	3.947E-009
450	9.350E+001	1.653E-009	1.157E-011	4.330E+014	1.671E-010	4.974E-003

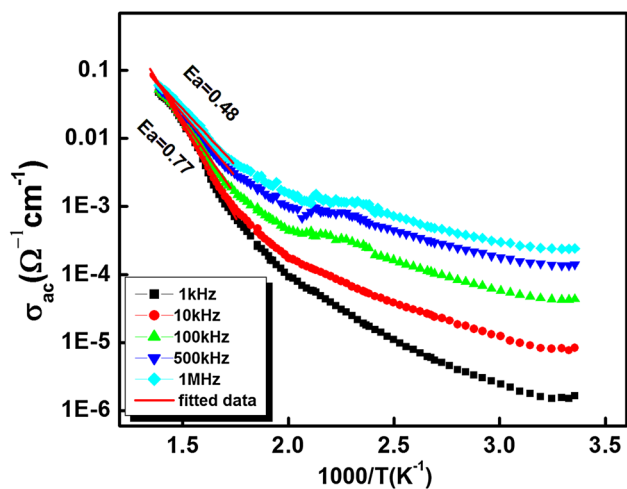


**Fig. 5** Temperature dependent AC conductivity spectrum at selected temperature (100–450 °C)

using the fitting data of  $\sigma_{ac}$  vrs temperature (Fig. 5). The  $E_a$  for 1 kHz, 10 kHz, 100 kHz, and 1 MHz are 0.48, 0.52, 0.63, 0.69, 0.77 respectively. The  $E_a$  value is lower in the region of low temperature that may be due to the hopping between localized states in a disordered manner of charge carriers [30–32].

### 3.5 Complex Modulus Analysis

Complex modulus is an another technique for establishing and providing information about the electrical properties

of the compound as well as to make a distinction against relaxation time, polarization, bulk properties, grain boundary conduction effects, happening in the modulus spectrum. The subsequent general relations of modulus [real ( $M'$ ) and Imaginary ( $M''$ ) part] technique can be calculated from the equation below:

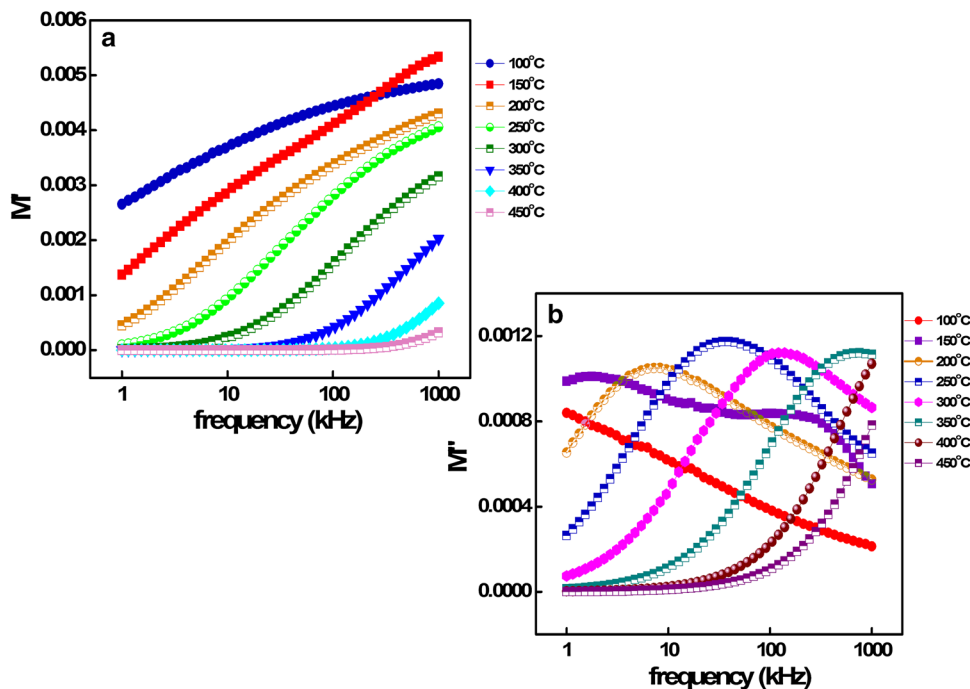
$$M' = A \left[ \frac{(\omega RC)^2}{1 + (\omega RC)^2} \right] = A \left[ \frac{\omega^2 \tau^2}{1 + \omega^2 \tau^2} \right] \tag{11}$$

$$M'' = A \left[ \frac{(\omega RC)}{1 + (\omega RC)^2} \right] = A \left[ \frac{\omega \tau}{1 + \omega^2 \tau^2} \right] \tag{12}$$

where  $A = \frac{C_0}{C}$  and other symbols have their usual meaning

Figure 6a, b displays the variation of modulus spectrum ( $M'$  and  $M''$ ) with frequency at different values of temperature. The real part of modulus decreases and attains zero towards the lower frequency region and at higher temperature, whereas with rise in the frequency the values reaches to an asymptotic value which can occur due to the existence of conduction mechanism and shorter mobility of charge carriers. Almost similar trend can be observed at different selected temperature, which implies the absence of non-Debye relaxation and electronic polarization mechanism in the synthesized compound [33]. From Fig. 6b it can be noticed that at higher frequency the peak of the  $M''$  tends to move towards it. At the region of high temperatures this phenomenon dominates due to the association of the relaxation mechanism with the hopping of charge carriers. The broadening of the asymmetric peak suggests the existence

**Fig. 6 a, b** Real and Imaginary part of Complex magnetic elastic constant variation with frequency at some selected temperature of  $\text{Bi}(\text{Co}_{2/3}\text{Nb}_{1/3})\text{O}_3$



of multiple relaxation time constants [34] and non-Debye of relaxation mechanism.

## 4 Conclusion

The compound BCN has been fabricated using high-temperature mixed oxide technique and by repeated firing the calcinations temperature is optimized. The prepared electronic compound have an orthorhombic structure that has been revealed from structural analysis obtained from room temperature XRD (X-ray diffraction) pattern. The electrical parameters of the BCN compound is both frequency and temperature dependent that can be obtained revealed from the experimental results. The electrical conductivity of the prepared compound analyzed from impedance spectroscopy is found to follows Jonscher's universal power law. The impedance characteristics of the compound signify the presence of non-Debye type of relaxation phenomena, grain and grain boundary effects, and subsistence of semiconducting nature (NTCR-type behaviour) in the sample. The complex modulus spectra of the specimen exhibits the presence of non-Debye type of relaxation. An proposed equivalent model demonstrated the occurrence of the electrical phenomenon inside the studied material. This lead-free prepared studied perovskite can be used in different applications including transducers, random access multi-state memories, data storage recorder, etc. which can be indicated by observing the experimental results of frequency–temperature variant capacitive (dielectric constant and loss) characteristics

## Compliance with Ethical Standards

**Conflict of interest** It is certified that the authors have no conflict of interest and this research work is original.

## References

1. Y. Konishi, Proc. IEEE **79**(6), 725 (1991)
2. J.K. Plourde, C.L. Ren, IEEE Trans. Microw. Theory Tech. **29**, 754 (1981)
3. S.N. Das, S.K. Pradhan, D.P. Kar, S. Bhuyan, R.N.P. Choudhary, J. Mater. Sci. Mater. Electron. **29**, 9375 (2018)
4. S.K. Pradhan, S.N. Das, S. Bhuyan, C. Behera, R. Padhee, R.N.P. Choudhary, Appl. Phys. A **122**, 604 (2016)
5. G. Martinelli, M.C. Carotta, M. Ferroni, Y. Sadaoka, E. Traversa, Sens. Actuators B **55**, 99 (1999)
6. J.R. Macdonald, Solid State Ion. **13**, 147 (1984)
7. S.K. Pradhan, S.N. Das, S. Halder, S. Bhuyan, R.N.P. Choudhary, J. Mater. Sci. Mater. Electron. **28**, 9627 (2007)
8. S. Halder, S. Bhuyan, S.N. Das, S. Sahoo, R.N.P. Choudhary, P. Das, K. Parida, Appl. Phys. A **123**, 781 (2017)
9. B. Jaffe, W.R. Cook, H. Jaffe, *Piezoelectric Ceramics* (Academic Press, London, 1971)
10. S.E. Park, T.R. Shrout, J. Appl. Phys. **82**, 1804 (1997)
11. S.N. Das, S.K. Pradhan, S. Bhuyan, R.N.P. Choudhary, J. Mater. Sci. Mater. Electron. **28**, 18913 (2017)
12. M. Gajek, S. Fusil, K. Bouzouhane, J. Fontcuberta, A. Barthelémy, A. Fertet et al., Nat. Mater. **6**, 296 (2007)
13. M. Bibes, A. Barthélémy, Nat. Mater. **7**, 425 (2008)
14. J.F. Scott, Nat. Mater. **6**, 256 (2007)
15. N. Klein, M. Schuster, S. Vitusevich, M. Winter, H.R. Yi, J. Eur. Ceram. Soc. **21**, 2687 (2001)
16. H. Tamura, T. Konoike, Y. Sakabe, K. Wakino, J. Am. Ceram. Soc. **67**, C59 (1984)
17. S. Halder, K. Parida, S.N. Das, S.K. Pradhan, S. Bhuyan, R.N.P. Choudhary, Phys. Lett. A **382**, 716 (2018)
18. H. Ogihara, C.A. Randall, S. Trolier-Mc Kinstry, J. Am. Ceram. Soc. **92**, 110 (2009)
19. C.C. Huang, D.P. Cann, X. Tan, N. Vittayakorn, J. Appl. Phys. **102**, 044103 (2007)
20. J.B. Lim, S. Zhang, N. Kim, T.R. Shrout, J. Am. Ceram. Soc. **92**, 679 (2009)
21. B. Park, *An Interactive Powder Diffraction Data Interpretation and Indexing Program Version 2.1* (E. WU School of Physical Sciences, Flinders University of South Australia, Adelaide, 1989)
22. A.L. Patterson, Phys. Rev. **56**, 978 (1939)
23. S.N. Das, A. Pattanaik, S. Kadambini, S. Pradhan, S. Bhuyan, R.N.P. Choudhary, J. Mater. Sci. Mater. Electron. **27**, 10099 (2016)
24. T.G. Reddy, B.R. Kumar, T.S. Rao, J.A. Ahmed, Int. J. Appl. Eng. Res. **6**, 571 (2011)
25. S.N. Das, S. Pradhan, S. Bhuyan, R.N.P. Choudhary, P. Das, J. Electron. Mater. **46**, 1637 (2016)
26. J. Plocharski, W. Wiczeoreck, Solid State Ion. **28**, 979 (1982)
27. A. Tripathy, S.N. Das, S.K. Pradhan, S. Bhuyan, R.N.P. Choudhary, J. Mater. Sci. Mater. Electron. **29**, 4770 (2018)
28. P. Gupta, R. Padhee, P.K. Mahapatra, R.N.P. Choudhary, J. Mater. Sci. Mater. Electron. **28**, 17344 (2017)
29. K. Jonscher, Nature **267**, 673 (1977)
30. S.K. Pradhan, S.N. Das, S. Bhuyan, C. Behera, R.N.P. Choudhary, J. Mater. Sci. Mater. Electron. **28**, 1198 (2017)
31. D.P. Almond, A.R. West, Solid State Ion. **11**, 57 (1983)
32. S. Upadhyay, A.K. Sahu, D. Kumar, O. Parkash, J. Appl. Phys. **84**, 828 (1998)
33. S. Halder, K. Parida, S.N. Das, S. Bhuyan, R.N.P. Choudhary, J. Mater. Sci. Mater. Electron. **28**, 15928 (2017)
34. S.N. Das, S.K. Pradhan, S. Bhuyan, S. Sahoo, R.N.P. Choudhary, M.N. Goswami, J. Electron. Mater. **47**, 843 (2017)